An evolutionary trade-off between parasite virulence and dispersal at experimental invasion fronts

Louise Solveig Nørgaard[1,2#*], Giacomo Zilio[2#], Camille Saade[2],

Claire Gougat-Barbera[2], Matthew D. Hall[1], Emanuel A. Fronhofer[2] & Oliver Kaltz[2*]

[1]School of Biological Sciences and Centre for Geometric Biology, Monash University, Melbourne 3800, Australia

[2]ISEM, University of Montpellier, CNRS, EPHE, IRD, Montpellier, France.

*Corresponding author: oliver.kaltz@umontpellier.fr; lnorga10@hotmail.com; [#]Shared first author contribution

Running title: An evolutionary trade-off at invasion fronts

Keywords: *Paramecium caudatum*, *Holospora undulata*, host-parasite interactions, experimental evolution, disease, epidemics, eco-evolution, range expansion, dispersal syndrome, horizontal and vertical transmission

Article type: Letter

Word count abstract: 148, Main text word count: 5607, References: 75, Figures: 5

Author contributions; OK, LN and GZ conceived the study. OK, LN, GZ, MH, and EAF helped design the experiments. LN, GZ, CGB and OK performed the experimental work., LN, GZ, MH, OK and EAF performed the statistical analysis. EAF, CS and OK developed, and CS analysed the epidemiological model. All authors interpreted the results and contributed to the writing of the manuscript.

Data accessibility: Data and code for the epidemiological model are available via Figshare: https://doi-org/10.6084/m9.figshare.12638957.v1

Competing interests: Authors have no competing interests.

Format: This manuscript is formatted to meet PNAS requirement for initial submission.

ABSTRACT

Changing environments and habitat structure likely affect eco-evolutionary processes involved in the spatial spread of disease. Exploitative parasites are predicted to evolve in highly connected populations or in expanding epidemics. However, many parasites rely on host dispersal to reach new populations, potentially causing conflict between local transmission and global spread. We performed experimental range expansions in interconnected microcosms of the protozoan *Paramecium caudatum*, allowing natural dispersal of hosts infected with the bacterial parasite *Holospora undulata*. Parasites from range front treatments were less virulent and interfered less with host dispersal, but also invested less in horizontal transmission than parasites from range cores. An epidemiological model fitted on experimental time-series data confirmed this trade-off between dispersal adaptation and transmission, so far rarely considered in theoretical models. Our study illustrates the importance of the ecology and evolution of dispersal-related traits in spatial non-equilibrium scenarios, including emerging diseases, metapopulations or biological invasions.

SIGNIFICANCE STATEMENT

What drives parasite evolution in spatially expanding epidemics? Many parasites require dispersal of infected hosts to reach new patches, and this may produce specific adaptations enhancing spatial spread. We performed experimental range expansions in an aquatic model system, with natural dispersal of infected hosts. Parasites from experimental range fronts were less virulent and interfered less with host dispersal, but also invested less in horizontal transmission than parasites from the range core. Thus, dispersal adaptation at the front may come at a cost of reduced horizontal transmission, a trade-off rarely considered in theoretical models on parasite virulence evolution. These results have important implications in the context of emerging diseases, and for parasite evolution during biological invasions or other spatial non-equilibrium scenarios.

INTRODUCTION

In an increasingly connected world, and with changing environments and habitats, we are facing the risk of infectious diseases spreading outside their natural range and over large geographic scales [1–5]. This issue is of concern to human health, agriculture and wildlife conservation, and understanding the ecological and evolutionary drivers represents a major challenge to epidemiologists and evolutionary biologists [6–8]. Due to their short generation time and large population sizes, parasites have the potential to evolve rapidly, and therefore one important question is whether changes in transmissibility or virulence already occur while an epidemic is progressing [9]. Classic theory predicts evolutionary optima for these traits only in large, spatially homogeneous populations at equilibrium [10,11], but these conditions are unlikely to be met during an epidemic [12,13]. In patchy real-world populations, parasites experience extinction-recolonization dynamics typical of metapopulations, with epidemic spread critically depending on population connectivity and the mobility and dispersal of infected hosts [14–19]. Although fundamental for epidemiology, it is still unclear how these spatio-temporal aspects affect concomitant evolutionary processes, and whether they might even lead to specific parasitic adaptations enhancing the spatial spread of the epidemic (see 20–22)

Recent theory has begun to develop a conceptual framework to investigate parasite evolution in spatially explicit, non-equilibrium settings [23]. Assuming a classic virulence-transmission trade-off [24,25] and local feedbacks between epidemiology and selection, several models predict that more virulent parasites will evolve in highly connected "small-world" landscapes [26–28] or at the front of advancing epidemics [20], where host exploitation and transmission is not limited by local depletion of susceptible hosts ("self-shading"). These predictions are consistent with observed changes in the predominance of a highly virulent honeybee virus at the front of progressing epidemics in New Zealand [29], and potentially also with observations for parasites and pathogens of amphibian species [30,31].

Yet, not all host-parasite systems show this pattern. For instance, the geographic spread of a bacterial pathogen of North American house finches was associated with decreased virulence in the newly invaded areas [32]. Likewise, in monarch butterflies, hosts that sustain long or frequent migrations were found to harbour less virulent parasites [33]. This may be explained by the way parasite dispersal enters

3

76   into the equation. Namely, if parasites travel with their infected hosts, exploitation of host resources

77   may reduce dispersal, thereby introducing a novel dispersal-virulence trade-off. Osnas et al. (2015)

78   show that such trade-off can lead to selection favouring more prudent and dispersal-friendly parasites

79   at the moving edge of an epidemic that escape more virulent and transmissible parasites from the core

80   of an epidemic. This latter idea mirrors classic principles from metapopulation theory and

81   metacommunity ecology, based on trade-offs between competitive ability and colonisation/dispersal

82   [20,34–36]. It also relates to recent work on invasive species and range expansions, where dispersal

83   evolution plays a key role in determining the rate of spatial diffusion [37]. In this sense, parasites may

84   evolve 'invasion syndromes', with characteristic changes in morphology, life history or transmission

85   strategies [30,31,38], thereby creating a positive feedback loop between rates of dispersal and rates of

86   spatial spread of infection.

87   Although the study of naturally expanding parasites remains the ultimate litmus test of the theory,

88   controlled experiments can verify important assumptions and serve as proof of principle [39]. For

89   example, we can manipulate demographic conditions in experimental microcosms to mimic the front

90   and core of an expanding epidemic [36] or artificially change levels of population mixing to study

91   epidemiological or evolutionary processes [39]. Indeed, studies of the latter type found that

92   experimentally shifting populations from local to global "dispersal" favoured more virulent parasites

93   [40–42], as predicted by theory [23,43]. Yin (1993) [44] further showed that phage diffusion on bacterial lawns

94   is associated with the appearance of faster replicating mutants in the periphery. However, to our

95   knowledge, there are no studies addressing experimental evolution of parasites from an explicit

96   metapopulation perspective, under natural dispersal of a host and its parasite.

97   For (micro-)organisms with directed movement, experimental landscapes can be created to study

98   metapopulation processes or range expansion dynamics with natural dispersal [45–47]. Here, we

99   employed such an approach to investigate the experimental evolution of spatially spreading parasites,

100 where all parasite dispersal is host-mediated. Using two-patch dispersal arenas for the ciliate

101 *Paramecium caudatum* infected with the bacterial parasite *Holospora undulata*, we mimicked a range

102 expansion scenario, with a front population of hosts (and parasites) dispersing into a new microcosm

4

103   during each selection event, and a core population constantly remaining in place (and losing

104   emigrants; see Fig. 1). After 55 episodes of dispersal selection, we then assayed evolved front and core

105   parasites under common garden conditions on naive hosts. Multiple traits were measured, namely the

106   parasites' effect on host dispersal, investment in horizontal transmission and their impact on host

107   replication and survival. We further obtained additional independent estimates of parasite traits by

108   fitting a simple epidemiological model to time series data (population density, infection prevalence)

109   from the experimental assay.

110   Because parasite persistence in the front populations depended entirely on host dispersal, we predicted

111   that front parasites would evolve minimal impact on host dispersal, or even increase dispersal of

112   infected hosts [48]. Such dispersal adaptations could involve a decrease in parasite virulence [22] and

113   generate an evolutionary trade-off with investment in horizontal transmission, not expected to occur in

114   the core populations. Our results were broadly consistent with these predictions, and we conclude that

115   differential dispersal selection pressures arising at the core and front of a range expansion can lead to

116   marked divergence of parasite life-history traits and the emergence of a 'parasite dispersal syndrome'.

117   **RESULTS**

118   Evolved parasites from the five front and five core selection lines were extracted and the inocula used

119   to infect naïve hosts (three genotypes). Several traits were measured for these newly infected assay

120   cultures (for timing of assays see Table S1 and statistical analyses Tables S2, S3).

121   **Infected host dispersal**

122   On average, hosts infected with front parasites dispersed twice as much (mean dispersal rate: $0.24 \pm$

123   0.05 SE x 3h^{-1}) as those infected with the core parasites (0.12 ± 0.02 SE; Fig. 2A), and this effect of

124   selection treatment was significant ($\chi_1^2 = 4.9$, p = 0.027; Table S2). The distribution of the differences

125   between model predictions for front and core treatments (small panel, Fig. 2A) also shows that higher

126   front-parasite dispersal is the most frequent predicted outcome (>98%; mean front-core difference:

127   0.12, 95% CI [0.08; 0.35]). This general trend was consistent on all three host genotypes tested (Fig.

128   S4; Table S3). Fig. S4 further shows that levels of front-parasite dispersal were similar to reference

129   data for uninfected hosts, whereas core parasites generally reduced host dispersal.

130 Using video analysis, we investigated variation in two parameters of *Paramecium* swimming

131 behaviour: swimming speed and trajectory variation (tortuosity). We found no evidence that infection

132 with core or front parasites had significant effects on these two parameters ($p > 0.25$; Table S2, neither

133 when tested on host genotypes individually S3; Fig S5, S6). Moreover, mean levels of swimming

134 speed or tortuosity were not significantly correlated with infected dispersal rates ($r \leq 0.15$, $n = 29$, $p >$

135 0.4), indicating that dispersal was not directly affected by these aspects of swimming behaviour (see

136 also path analysis below).

137 **Parasite life-history traits**

138 **Infectivity.** Measurements of infection prevalence early after inoculation (day 4) inform on parasite

139 horizontal transmission potential (infectivity). Core parasites had slightly higher infection success

140 (selection line average proportion of infected hosts: 0.59 ± 0.05 SE) than front parasites (0.51 ± 0.03

141 SE; Fig. 2B). Although not formally significant (effect of selection treatment: $\chi_1^2 = 2.43$, $p = 0.118$;

142 Table S2; predictive difference distribution front-core infectivity: mean = -0.08, CI [0.02; -0.18]; Fig

143 2B; see also Fig. S7 for genotype specific responses), this trend was consistent with higher estimates

144 of the transmission parameter for core parasites in an epidemiological model fitted to our experimental

145 data (see below; Fig. 4).

146 **Investment in horizontal transmission (infectiousness).** It takes several days until infected hosts

147 produce horizontal transmission stages and become infectious. In our assay, the first infectious hosts

148 appeared on day 6 p.i., and their frequency then increased over the following week, reaching up to

149 100% (Fig. 2C). Over this period, populations infected with front parasites produced a lower

150 proportion of infectious hosts (mean: 0.41 ± 0.03 SE) than did populations infected with core parasites

151 (0.53 ± 0.03 SE; effect of selection treatment: $\chi_1^2 = 13.2$, $p < 0.001$; Table S2; predictive difference

152 distribution front-core infectiousness: mean = -0.10; CI [0.04; -0.23]; Fig. 2C). There was also a

153 difference in timing: on average, core parasites produced the first infectious hosts c. 1 day earlier than

154 did front parasites (day 6 vs day 7) and subsequently showed a faster increase in the proportion of

155 infectious hosts (treatment x time interaction: $\chi_1^2 = 13.54$, $p < 0.001$, Table S2; Fig. 2C). These

156 differences in total investment and/or timing broadly hold on all three host genotypes tested (Table S3;

157 Fig. S8).

158 **Virulence.** We isolated single infected individuals from the core and front infected assay cultures and

159 measured the impact of infection on host division and survival over a 20-day period. Exposed, but

160 uninfected, controls were isolated from the same assay cultures and run in parallel.

161 *Host division.* By day 10, 87% of the infected singletons had accomplished at least one division (266 /

162 305 replicates; mean maximum cell number observed over this period: 8.5 ± 0.6 SE). Analysis of

163 maximum cell density revealed a significant selection treatment x infection status interaction ($\chi_1^2 =$

164 16.9, p > 0.001; Table S2). Namely, hosts infected with front parasites reached nearly twice as high

165 maximum densities (10.9 ± 1.3 SE) than those infected with core parasites (5.9 ± 0.9 SE; contrast front

166 vs core: $t_{601} = 4.7$, p < 0.0001; predictive difference distribution front-core: mean = 4.6, CI [1.4; 9.6];

167 Fig. 3A).

168 *Host survival.* As for host division, there was a significant selection treatment x infection status

169 interaction for host survival ($\chi_1^2 = 7.4$, p = 0.006; Table S2). By day 20, infections with front parasites

170 had experienced a 50% lower mortality (mean proportion of infected replicates extinct: 0.19 ± 0.05

171 SE) than infections with core parasites (0.37 ± 0.1 SE; contrast front vs core: $t_{601} = 3.75$, p > 0.001;

172 predictive difference distribution front-core: mean = 0.30, CI [0.04;0.62]; Fig. 3B). Moreover, effects

173 on host division and on host survival were positively correlated: parasites which allowed more host

174 division also allowed higher host survival (means per parasite selection line: $r = 0.84 \pm 0.19$, n = 10, p

175 = 0.003). Thus, core parasites generally had negative effects, whereas front parasites only had little, or

176 even positive, impact on their hosts reproduction and survival (Fig. 3A and 3B), and these opposing

177 trends were consistent across the three host genotypes tested (Table S2; Fig. S9 & S10).

178 **Path analysis**

179 Using path analysis, we explored the direct and indirect contributions of different traits to the observed

180 variation in infected host dispersal (Fig. 4A). Host division (= maximum cell density) was the only

181 trait with a significant direct effect on host dispersal ($F_{1,20} = 6.16$, p = 0.022; Fig. 3B); thus, lower

182 virulence was associated with higher dispersal rates of infected hosts. Horizontal transmission

183 investment (= cumulative infectiousness) had a moderate indirect effect on dispersal via its significant

184 negative relationship with virulence ($F_{1,23}$ = 4.47, p = 0.0456; Fig. 3C). Swimming behaviour (speed,

185 tortuosity) had no significant direct effect on dispersal, and were themselves only very marginally

186 affected by virulence or infectiousness (Fig. 4A).

187 **Epidemiological model fits**

188 By fitting an epidemiological model to the population-level data from the assay replicate cultures

189 (infection prevalence and population density), we obtained independent estimates of parasite

190 parameters. In the model, we integrated the basic features of the infection life cycle, assuming simple

191 population growth and regulation (Beverton-Holt type model, 49) and parameterising virulence as the

192 reduction in host fecundity.

193 The model captured the main trends in the demographic and epidemiological dynamics observed in

194 the cultures. This is illustrated in Fig. 5A, showing the model fits for the densities of infected and

195 uninfected hosts for the 63D host genotype (for the other two host genotypes, see SI 4, Fig. S11).

196 Parameter estimates confirm the main trends found in our experimental assays. Namely, the model fits

197 show that front parasites have lower virulence, lower transmission rate and longer latency time than

198 core parasites (Fig. 5B-D), a pattern largely consistent for the three host genotypes tested (Fig. S11).

199 **DISCUSSION**

200 In times of global epidemics [1,4,32] it is important to know how parasites evolve while spreading through

201 a landscape or entire continents. Recent theory suggests that spatial 'viscosity' and connectedness

202 generate eco-evolutionary feedbacks, with important consequences for parasite virulence evolution

203 and the speed of epidemics [23]. However, so far little attention has been given to the fact that many

204 parasites travel together with their dispersing hosts, which may considerably affect evolutionary

205 predictions [22,28,48].

206 To address this issue, we performed a simplified range expansion experiment, with natural dispersal of

207 infected hosts. Our 'range front' and 'range core' treatments imposed differential selection on host

208   dispersal (see 52) and resulted in divergent parasite phenotypes: front parasites allowed for higher

209   dispersal of their infected hosts, were less virulent and showed reduced investment in horizontal

210   transmission, compared to the parasites from the core selection treatment. These patterns were largely

211   robust between the three naive host genotypes tested, and additionally confirmed by results from an

212   epidemiological model that we fitted to time-series data obtained from our assay cultures.

213   *Evidence for a virulence - dispersal trade-off*

214   Our experimental result of multi-trait changes joins empirical observations of "invasion syndromes" in

215   naturally spreading diseases, such as avian malaria in Europe [51] or lungworms of invasive cane toads

216   in Australia [30]. Lungworms at the invasion front, for example, exhibit distinct life-history traits

217   (reduced age at maturity, larger infective and free-living larvae), possibly representing adaptations to

218   invasion history [30]. We replayed such an invasion history, by mimicking the spatial progression of an

219   isolated population in our range front treatment, which was expected to favour parasites that succeed

220   in dispersing together with their infected hosts. This explains why our front parasites were found to

221   facilitate higher host dispersal. Importantly, higher host dispersal was associated with higher host

222   replication and survival, indicating a dispersal - virulence trade-off (Fig. 2 and 3). Reduced virulence,

223   in turn, was associated with reduced horizontal transmission potential (Fig. 2C), consistent with

224   previous findings in this system [52–54] and reflects a virulence-transmission trade-off for this parasite.

225   Thus, we conclude that the evolution of higher parasite dispersal in front parasites came at the cost of

226   reduced horizontal transmission, a trade-off resulting from a reduction in virulence.

227   The idea that parasite exploitation strategies can be shaped by the interplay between local transmission

228   and global dispersal was formalised in a theoretical model by Osnas et al. (2015). They showed that

229   implementing a trade-off between virulence and the capacity of infected hosts to disperse, favours less

230   virulent strains at the front of an epidemic, escaping the more competitive (and more virulent) strains

231   through faster dispersal [22]. Such a selection scenario may explain observed geographic patterns of

232   virulence for a bacterial pathogen of North American house finches [32], and it is qualitatively consistent

233   with our results.

234   *Trait relationships: Proximate causes of infected dispersal rate*

9

235 Just like parasites can alter their hosts behaviour to increase transmission [55], they may also evolve to

236 manipulate host dispersal [48,56]. However, we find little evidence for manipulation to increase the

237 dispersal. Consistent with previous observations of negative effects of infection in this [57] and other

238 systems [36,58–60], core parasites reduced host dispersal, whereas infection with front parasites produced

239 levels of dispersal comparable to uninfected *Paramecium*. Path analysis indicates that virulence is the

240 main direct predictor of host dispersal in our assays. Investment in horizontal transmission had an

241 indirect effect via decreased virulence. Although intuitively straightforward through a weakening of

242 infected hosts, the mechanistic link between virulence and dispersal remains unclear. We found no

243 effect of infection on swimming behaviour, nor was there a direct link between swimming behaviour

244 and dispersal, which is frequently observed in other protists [47]. Possibly, infection influences other

245 dispersal-relevant traits, such as the vertical distribution in the water column [61,62], determining the

246 proximity of individuals to the opening that leads to the other tube in the dispersal arena (see Fig. 1).

247 *Contrasting scenarios: Dispersal to new sites vs access to new hosts*

248 While our results suggest more prudent parasites might be spreading at invasion fronts, other

249 theoretical models and experiments reach opposite conclusions. Griette et al. (2015), for example,

250 predict highest levels of virulence at the front of an epidemic wave, where transmission is not limited

251 by the availability of susceptible hosts, thereby favouring the most 'rapacious' variants. Following this

252 line of argument, experiments with viruses and bacteriophages have studied virulence evolution by

253 artificially manipulating dispersal or population connectivity [40–42]. Kerr et al. (2006) pipetted bacteria

254 and phage either to adjacent wells or to more distant wells on a multi-well plate, in analogy to our

255 'core' and 'front' treatments [41]. Contrary to our results, their latter treatment of unrestricted dispersal

256 resulted in the evolution of more virulent phages, confirming the prediction that erosion of spatial

257 structure in 'small worlds' favours more transmissible and more virulent parasites [27,28,63].

258 One reason for these contrasting results is that in Kerr et al. (2006), dispersal was artificial and cost-

259 free, eliminating a possible virulence-dispersal trade-off. Secondly, our experiment considered a

260 different spatial scenario where infected hosts disperse into empty space, more characteristic of a

261 biological invasion. This means that higher dispersal was not rewarded with more access to

262 susceptible hosts, as assumed in the above models [20,63]. Future experiments can test whether we still

263 find reduced virulence in the front selection treatment, if infected hosts disperse into patches already

264 occupied by uninfected hosts.

265 Taken together, these examples illustrate the different ways in which spatial spread and dispersal of

266 parasites can be approached both conceptually and experimentally, with very different evolutionary

267 outcomes. We argue that particular attention should be given to *how* parasites disperse through a

268 landscape, namely because dispersal itself may be the target of selection [22,36].

269 **More vertical transmission at invasion fronts?**

270 We used the replication of infected hosts as a measure of virulence. However, for this parasite, host

271 replication is also equivalent to vertical transmission, because reproductive stages are passed on to

272 daughter cells during mitosis. In this sense, parasites in our front selection treatment underwent a shift

273 from horizontal transmission towards higher levels of vertical transmission. This is due to an

274 underlying developmental trade-off, where reduced conversion of reproductive into infective stages

275 decreases the negative effects on host replication [54,64], but simultaneously reduces horizontal

276 transmission capacity.

277 Magalon et al. (2010) observed a similar increase in the efficacy of vertical transmission of this

278 parasite in frequently disturbed populations [53]. In fact, their study can be re-interpreted as a range

279 expansion experiment, with the disturbance treatment mimicking the frequent recolonization events

280 occurring at the front [65] and the less disturbed control treatment reflecting more stable conditions in

281 the core (see Fig. 1 in 55). The explanation for the evolutionary shift towards vertical transmission is

282 that the demographic oscillations at the invasion front, with frequent periods of low host density and

283 high host fecundity, increase the contribution of vertical transmission to the total transmission success

284 [66]. Because vertical transmission is a means of 'reproductive insurance', we would generally expect it

285 to evolve in association with parasite dispersal syndromes in expanding populations or in highly

286 disturbed habitats [67]. We note, however, that in our present experiment both core and front populations

287 went through density bottlenecks, making the dispersal constraint the main selective driver.

Conclusions

Our results show that different segments of an epidemic wave may be under divergent selection

pressures. Namely, we find evidence that dispersal selection at an experimental invasion front leads to

reduced virulence. This contrasts with observations in certain natural epidemics [29,30], while confirming

others [32,33]. This calls for more detailed investigations of the role of dispersal for epidemic spread and

its implications for the evolution of parasite life-history traits. Our relatively simple statistical

modelling exercise suggests that time series data from natural populations represent a useful resource

for such a challenge. Establishing a better understanding of the interaction between demography and

rapid evolutionary change in spreading populations is crucial for the management of emerging

infectious diseases and disease outbreak in the wild, biological invasions and other non-equilibrium

scenarios.

MATERIALS AND METHODS

Study system

Paramecium caudatum is a filter-feeding freshwater protozoan ciliate from still water bodies in the

Northern Hemisphere [68]. It has a germline micronucleus and a somatic macronucleus. Our cultures are

maintained asexually in a lettuce medium with the food bacterium *Serratia marcescen*s at 23°C,

allowing 1-2 population doublings per day [69]. The gram-negative alpha-proteobacterium *Holospora*

undulata infects the micronucleus of *P. caudatum*, and can be transmitted both horizontally (by s-

shaped infective spores, 15 µm) upon host death or during cell division, and vertically, when

reproductive bacterial forms (5 µm) segregate into daughter nuclei of a mitotically dividing host [70].

After ingestion by feeding *Paramecium,* infective spores invade the micronucleus, where they

differentiate into the multiplying reproductive forms. After one week, reproductive forms begin to

differentiate into infective spores [61,69]. Infection with *H. undulata* reduces host cell division and

survival [54] and also host dispersal [57].

Long-term experiment

Similar to Fronhofer and Altermatt (2015), we imposed dispersal selection in 2-patch microcosm

arenas (Fig. 1, see also SI 1), built from two 14-mL plastic tubes, interconnected by 5-cm silicon

tubing, which can be blocked using a clamp (see Fig. S1). We define dispersal as the active swimming

of *Paramecium* from one microcosm to the other via the connective tuber (i.e., the dispersal corridor).

The experiment was seeded from an uninfected host line ("63D", haplotype B) from our laboratory

that had been under "core selection" (see below) for three years and shows characteristically low

dispersal propensity (O.K., unpublished data). This 63D mass culture was infected with an inoculum

of *H. undulata* prepared from a mix of various infected stock cultures (for details, see SI 2). All

parasites in this mix originate from a single isolate of *H. undulata* established in the lab in 2001.

In the front selection treatment, we placed *Paramecium* in one tube ("core patch") and opened the

connection for three hours, allowing them to swim into the other tube ("front patch"). *Paramecium*

from the front patch were recovered and cultured in bacterised medium, allowing for natural host

population growth and parasite transmission. After one week, we imposed another dispersal episode,

again recovering only the *Paramecium* from the front patch, and so on. The core selection treatment

followed the same alternation of dispersal and growth periods, except that only *Paramecium* from the

core patch were recovered and propagated (Fig. 1, and SI 1). We established five infected 'core

selection' lines and five infected 'front selection' lines that were maintained for a total of 55 cycles of

dispersal. To minimise potential effects of host (co)evolution, we extracted infectious forms from each

selection line after cycle 30, inoculated a new batch of naïve 63D hosts and continued the experiment

for another 25 cycles. For details of the experimental protocols, see SI 1.

Parasite assays

At the end of the selection experiment, we extracted parasites from core and front selection lines to

inoculate new, naïve hosts. We then assayed parasite effects on host dispersal, infection life-history

and virulence. To obtain a general picture of trait expression, we tested the evolved parasites on naïve

63D hosts (same genotype as used in long-term experiment), as well as on two additional genotypes,

C023 (haplotype A, origin Germany) and C173 (haplotype B, origin Greece, both strains provided by

S. Krenek, TU Dresden, Germany). These two strains are highly susceptible to infection (O. Kaltz,

unpubl. data) but belong to two intra-specific clades that likely separated >10 MY ago (L. Bright,

341 SUNY, US, unpubl. data). Note that companion assays of evolutionary adaptations arising in the host

342 are reported elsewhere [50].

343 All assays were performed on a cohort of infected replicate cultures, over the course of three weeks

344 under common-garden conditions (Table S1). To initiate the cultures, we placed ≈ 5 x 10^3 cells of a

345 given naïve host genotype in 1.4 mL of bacterised medium in a 15-mL tube, to which we added the

346 freshly prepared inoculum of a given evolved parasite line (≈ 1.5 x 10^6 infectious spores, on average).

347 On day four post-inoculation (p.i.), when infections had established, we split the cultures into three

348 technical replicates and expanded the volume to 30 mL, by adding bacterised medium. A total of 90

349 replicate cultures were set up (2 selection treatments x 5 parasite selection lines x 3 host genotypes 3

350 technical replicates).

Dispersal of infected hosts

352 From day 14 to 19 p.i., we assayed dispersal rates of hosts infected with core and front parasites, using

353 linear 3-patch arenas where the *Paramecium* disperse from the middle tube to the two outer tubes (Fig.

354 S2). Arenas were filled with ~2800 individuals in the middle tube and after 3 h of dispersal, we

355 subsampled the middle tube (0.5 mL) and the pooled two outer tubes (3 mL) to estimate the number of

356 non-dispersers and dispersers under a dissecting microscope. Furthermore, from $\approx$20 arbitrarily picked

357 individuals stained with 1% lacto-aceto orcein (LAO fixation; Fokin and Görtz, 2009) we determined

358 the proportion of infected dispersers and non-dispersers (phase-contrast, 1000x magnification), from

359 which we then calculated the dispersal rate of infected hosts for each replicate culture (number of

360 dispersed infected hosts / total number of infected hosts per 3 h). Each of 88 available replicate

361 cultures was tested once. For statistical analysis, we excluded 13 replicates with very low population

362 density and/or infection prevalence (<10%), which prevented accurate estimation of dispersal of

363 infected individuals. Dispersal was not significantly affected by assay date ($\chi_2^2 = 2.56$, $p > 0.25$), and

364 this factor was therefore omitted from further analysis.

Parasite life-history traits

366 Infectivity. On day 4 p.i., we estimated infection prevalence in the 30 inoculated cultures, using LAO

367 fixation of ≈20 individuals, as described above. This measurement describes 'parasite infectivity', i.e.,

368 the capacity to successfully establish infections [61].

369 Epidemiology and parasite development. From day 6 to 13 p.i., we tracked population density and

370 infection prevalence in the 90 replicate cultures, using a blocked sliding window (day 6-8, 11-13) such

371 that each parasite x host genotype combination was measured once per day. As infections developed,

372 we also tracked changes in the proportion of infectious hosts, when reproductive forms are converted

373 into infective spores. These data were used for the fitting of an epidemiological model (see below).

374 Furthermore, we specifically compared core and front parasites for their levels of infectiousness (=

375 proportion of infectious hosts) between day 6 and day 11 p.i.. This time window describes the timing

376 and level of investment into horizontal transmission by the initial cohort of infected hosts [69].

377 Virulence. Early after inoculation of the initial 30 assay cultures (day 4 p.i.), we isolated single

378 infected and uninfected individuals from each culture and let them multiply for 9 days in 2-mL tubes

379 under permissive common-garden conditions. From these small monoclonal cultures, we started the

380 virulence assay by placing single individuals in PCR tubes filled with 200 μL of medium. We assessed

381 cell division on day 2 and 3 (visual inspection), on day 10 (from 50-μL samples) and on day 20 from

382 the total volume. A total of 645 replicates were set up, with 8-12 infected and uninfected replicates

383 from each of 28 of the 30 assay cultures. For further details, see SI 2 and Fig. S3.

384 Swimming behaviour. From the above monoclonal lines, we placed 200-μL samples (containing 10-20

385 individuals) on a microscope slide and recorded individual movement trajectories using a Perfex

386 SC38800 camera (15 frames per second; duration 10 s). For each sample, the mean net swimming

387 speed and swimming tortuosity (standard deviation of the turning angle distribution, describing the

388 extent of swimming trajectory change) was determined, using the BEMOVI package [72]. This assay

389 was performed for infected and uninfected monoclonal lines from 29 assay cultures, with 1-2 samples

390 per monoclonal line (106 replicates in total).

391 *Statistical analysis*

392 Statistical analyses were performed in R (ver. 3.3.3; R Development Core Team, available at www.r-

393 project.org) and in JMP (SAS Institute Inc. (2018) JMP®, Version 14, N.C.). To analyse variation in

394 parasite traits, we used generalised linear mixed-effect models [73]. Binomial error structure and logit

395 link were used for analysis of infected host dispersal (proportion dispersers), infectivity (proportion

396 infected individuals on day 4 p.i.), and horizontal transmission investment (proportion infectious hosts

397 day 6-11 p.i.). Normal error structure was used for analysis of swimming speed and tortuosity. For the

398 virulence assay, we analysed variation in host division (= maximum cell density per replicate; Poisson

399 error structure and log link) and survival (= replicate alive / dead on day 20; binomial error structure

400 and logit link).

401 In all analyses, parasite selection treatment (front vs core) was taken as a fixed effect and host

402 genotype and parasite selection line identity as random factors. Day p.i. was integrated as a covariate

403 in the analysis of infectiousness. In the virulence analyses, replicate infection status (infected /

404 uninfected) was included as a fixed factor. Analysis of variance (type II) was used to test for

405 significance of fixed effects (car package; Fox and Weisberg, 2018). In complementary comparisons,

406 we used ANOVA model predictions (and their variance) for core and front treatments to establish

407 predictive distributions of the front-core difference (e.g. Fronhofer *et al.*, 2017). For these

408 distributions, we calculated the mean difference and confidence intervals. Finally, we performed

409 multiple regressions (path analysis) to assess how infected host dispersal was affected by the

410 following traits: horizontal transmission investment (HTI, area under the curve of the proportion of

411 infectious hosts from day 6 - 11 p.i.), virulence (infected host division) and swimming behaviour

412 (tortuosity and net swimming speed). This analysis was based on trait means for 25 combinations of

413 parasite selection line and host assay genotype. To meet assumptions of normality, certain trait means

414 were transformed ($\log_2$ for host division, arcsine for dispersal, square root for HTI). To correct for

415 overall effects of host genotype, we first fitted univariate analyses for each trait, and then performed

416 the regressions on the residuals. Standardised beta regression coefficients were taken as path

417 coefficients.

418 *Epidemiological model fitting*

16

419 We fitted a simple epidemiological model to the above population density and infection prevalence

420 data recorded in our assay replicate cultures (day 6-13 p.i.). The aim was to obtain additional

421 independent estimates of parasite parameters (Table 1), namely virulence, but also the transmission

422 parameter or latency time, i.e. the time to onset of production of infectious forms (Rosenbaum et al.,

423 2019).

424 Model structure. We model the density of uninfected (S) and infected (I) hosts using ordinary

425 differential equations (ODEs). In the absence of parasites, we consider that uninfected *Paramecium*

426 growth follows the continuous time version of the Beverton-Holt model [49].

427 $$\frac{dS}{dT} = \left(\frac{b}{1+\alpha N} - d\right)S \tag{1}$$

428 where b is the birth rate, d the death rate and α the competition term. N is the total number of

429 individuals ($S + I$), which is equal to S in the absence of the parasite. In the presence of infected

430 individuals, uninfected individuals become infected at a rate proportional to the number of infected

431 and uninfected individuals at a rate β:

432 $$\frac{dS}{dT} = \left(\frac{b}{1+\alpha N} - d\right)S - \beta SI \tag{2}$$

433 $$\frac{dI}{dT} = \beta SI \tag{3}$$

434 Moreover, infected individuals also display Beverton-Holt dynamics, but their birth rate can be

435 decreased, hence we multiply b by a term $(1 - v)$, where v is the virulence of the parasite:

436 $$\frac{dS}{dT} = \left(\frac{b}{1+\alpha N} - d\right)S + \beta SI \tag{4}$$

437 $$\frac{dI}{dT} = \left(\frac{b(1-v)}{1+\alpha N} - d\right)I + \beta SI \tag{5}$$

438 Finally, vertical transmission of the parasite is not necessarily 100%, and some of the *Paramecium*

439 "born" from infected individuals could be free of parasites due to incomplete vertical transmission. We

440 name γ the proportion of successful vertical transmission:

441 $$\frac{dS}{dT} = \left(\frac{b}{1+\alpha N} - d\right)S - \beta SI + \left(\frac{b(1-v)}{1+\alpha N}\gamma\right)I \tag{6}$$

442 $$\frac{dI}{dT} = \left(\frac{b(1-v)}{1+\alpha N}\gamma - d\right)I + \beta SI \tag{7}$$

443   Since the majority of infected individuals were not yet producing infectious forms at the beginning of

444   the time series, we added another parameter, τ, which is the latency before an infected individual

445   becomes infectious (i.e., capable of horizontal transmission):

446    $$\beta = 0 \; if \; time < \tau \tag{8}$$

447   Model Fitting. We fitted the epidemiological model to the data using Bayesian inference and the *rstan*

448   R package (version 2.19.2). Using data from previous experiments (O. Kaltz, unpublished data), we

449   first fitted the Beverton-Holt model (Eq. 1) to growth curves of uninfected populations to estimate the

450   distributions of *b, d* and α for each host genotype. These distributions were used as priors for fitting

451   the full model (Eq. 6, 7, 8) on infection data. The model was fitted separately for each of the six

452   combinations of host genotype and parasite selection treatment. For simplicity, we fitted a single set of

453   parameters (*b, d,* α*, b,* β*,* γ*,* τ) over the different selection lines (with different initial conditions fitted

454   over each line). Priors distributions can be found in Table 1. Apart from *b,* d and α, we used lowly

455   informative priors that largely encompass expected values (*v* and γ priors are uniform over possible

456   values, τ prior is uniform over previously observed latency values, β prior follows a lognormal

457   distribution an order of magnitude wider than expected values). Fits were realized using the No U-

458   Turn Sampler (NUTS) with default rstan values and multiple chains (three chains per fit, each of total

459   length: 15 000 and warm-up length: 5 000).

460   **Table 1**. Model parameters, their signification and the priors used for fitting.

Parameters	Term	Priors
b	Birth rate	Posteriors from fitting eq. (1) on non-infected population data
d	Death rate	
α	Intraspecific competition coefficient	
v	Virulence (decrease in b)	Uniform (0, 1)
β	Horizontal transmission rate	Lognormal (-5, 0.9)
γ	Vertical transmission rate	Uniform (0.5, 1)
τ	Latency time	Uniform (144, 240)

461

REFERENCES

1. Bahl, J. *et al.* Temporally structured metapopulation dynamics and persistence of influenza A H3N2 virus in humans. *Proc. Natl. Acad. Sci. U. S. A.* **108**, 19359–19364 (2011).

2. Pettersson, J. H. O. *et al.* Re-visiting the evolution, dispersal and epidemiology of Zika virus in Asia article. *Emerg. Microbes Infect.* **7**, 1–8 (2018).

3. Findlater, A. & Bogoch, I. I. Human mobility and the global spread of infectious diseases: a focus on air travel. *Trends Parasitol.* **34**, 772–783 (2018).

4. Chinazzi, M. *et al.* The effect of travel restrictions on the spread of the 2019 novel coronavirus (COVID-19) outbreak. *Proc. 20th USENIX Secur. Symp.* **6 March**, 395–410 (2020).

5. Tatem, A. J., Rogers, D. J. & Hay, S. I. Global transport networks and infectious disease spread. *Adv. Parasitol.* **62**, 293–343 (2006).

6. Parratt, S. R., Numminen, E. & Laine, A.-L. Infectious disease dynamics in heterogeneous landscapes. *Annu. Rev. Ecol. Evol. Syst.* **47**, 283–306 (2016).

7. Penczykowski, R. M., Laine, A. L. & Koskella, B. Understanding the ecology and evolution of host-parasite interactions across scales. *Evol. Appl.* **9**, 37–52 (2016).

8. Clark, N. J. *et al.* Climate, host phylogeny and the connectivity of host communities govern regional parasite assembly. *Divers. Distrib.* **24**, 13–23 (2018).

486   9.   Holmes, E. C., Dudas, G., Rambaut, A. & Andersen, K. G. The evolution of Ebola

487   virus: Insights from the 2013-2016 epidemic. *Nature* **538**, 193–200 (2016).

488   10.   Cressler, C. E., McLeod, D. V., Rozins, C., Van Den Hoogen, J. & Day, T. The

489   adaptive evolution of virulence: a review of theoretical predictions and empirical tests.

490   *Parasitology* **143**, 915–930 (2016).

491   11.   Alizon, S., Hurford, A., Mideo, N. & Van Baalen, M. Virulence evolution and the

492   trade-off hypothesis: History, current state of affairs and the future. *J. Evol. Biol.* **22**,

493   245–259 (2009).

494   12.   Andre, J.-B. & Hochberg, M. E. Virulence evolution in emerging infectious diseases.

495   *Evolution (N. Y).* **59**, 1406–1412 (2005).

496   13.   Gandon, S. & Day, T. Evolutionary Epidemiology and the Dynamics of Adaptation.

497   *Evolution (N. Y).* **63**, 826–838 (2009).

498   14.   Keeling, M. J. *et al.* Dynamics of the 2001 UK Foot and Mouth epidemic: Stochastic

499   dispersal in a heterogeneous landscape. *Sci. New Ser.* **294**, 813–817 (2001).

500   15.   Viboud, C. *et al.* Synchrony, waves, and spatial hierarchies in the spread of influenza.

501   *Science (80-.).* **312**, 447–451 (2006).

502   16.   Dudas, G. *et al.* Virus genomes reveal factors that spread and sustained Ebola

503   epidemic. *Physiol. Behav.* **544**, 309–315 (2017).

504   17.   Ferrari, M. J. *et al.* The dynamics of measles in sub-Saharan Africa. *Nature* **451**, 679–

505   684 (2008).

506   18.   North, A. R. & Godfray, H. C. J. The dynamics of disease in a metapopulation: The

507   role of dispersal range. *J. Theor. Biol.* **418**, 57–65 (2017).

508   19.   Jousimo, J. *et al.* Ecological and evolutionary effects of fragmentation on infectious

509   disease dynamics. *Science (80-.).* **344**, 1289–1293 (2014).

510   20.   Griette, Q., Raoul, G. & Gandon, S. Virulence evolution at the front line of spreading

511   epidemics. *Evolution (N. Y).* **69**, 2810–2819 (2015).

512   21.   Leventhal, G. E., Hill, A. L., Nowak, M. A. & Bonhoeffer, S. Evolution and emergence

513   of infectious diseases in theoretical and real-world networks. *Nat. Commun.* **6**, (2015).

514   22.   Osnas, E. E., Hurtado, P. J. & Dobson, A. P. Evolution of pathogen virulence across

515   space during an epidemic. *Am. Nat.* **185**, 332–342 (2015).

516   23.   Lion, S. & Gandon, S. Evolution of spatially structured host-parasite interactions. *J.*

517   *Evol. Biol.* **28**, 10–28 (2015).

518   24.   Bull, J. J. Virulence. *Evolution (N. Y).* **48**, 1423–1437 (1994).

519   25.   May, R. M. & Anderson, R. M. Epidemiology and genetics in the coevolution of

520   parasites and hosts. *Proc. R. Soc. London - B. Biol. Sci.* **219**, 281–313 (1983).

521   26.   Boots, M., Hudson, P. J. & Sasaki, A. Large shifts in pathogen virulence relate to host

522   population structure. *Science (80-.).* **303**, 842–844 (2004).

523   27.   Kamo, M. & Boots, M. The evolution of parasite dispersal, transmission, and virulence

524   in spatial host populations. *Evol. Ecol. Res.* **8**, 1333–1347 (2006).

525   28.   Kamo, M., Sasaki, A. & Boots, M. The role of trade-off shapes in the evolution of

526   parasites in spatial host populations: An approximate analytical approach. *J. Theor.*

527   *Biol.* **244**, 588–596 (2007).

528   29.   Mondet, F., de Miranda, J. R., Kretzschmar, A., Le Conte, Y. & Mercer, A. R. On the

529   front line: Quantitative virus dynamics in honeybee (Apis mellifera L.) colonies along

530   a new expansion front of the parasite Varroa destructor. *PLoS Pathog.* **10**, e1004323

531   (2014).

532   30.   Kelehear, C., Brown, G. P. & Shine, R. Rapid evolution of parasite life history traits on

533   an expanding range-edge. *Ecol. Lett.* **15**, 329–337 (2012).

534   31.   Phillips, B. L. & Puschendorf, R. Do pathogens become more virulent as they spread?

535   Evidence from the amphibian declines in Central America. *Proc. Biol. Sci.* **280**,

536   20131290 (2013).

537   32.   Hawley, D. M., Osnas, E. E., Dobson, A. P., Hochachka, W. M. & Ley, D. H. Parallel

538   patterns of increased virulence in a recently emerged wildlife pathogen. *PLoS Biol.* **11**,

539   e1001570 (2013).

540   33.   De Roode, J. C., Pedersen, A. B., Hunter, M. D. & Altizer, S. Host plant species affects

541   virulence in monarch butterfly parasites. *J. Anim. Ecol.* **77**, 120–126 (2008).

542   34.   Calcagno, V., Mouquet, N., Jarne, P. & David, P. Coexistence in a metacommunity:

543   the competition-colonization trade-off is not dead. *Ecol. Lett.* **9**, 897–907 (2006).

544   35.   Oliveri, I., Michalakis, Y. & Gouyon, P.-H. Metapopulation Genetics and the

545   Evolution of Dispersal. *Am. Soc. Nat.* **146**, 202–228 (1995).

546   36.   Nørgaard, L. S., Phillips, B. L. & Hall, M. D. Infection in patchy populations:

547   Contrasting pathogen invasion success and dispersal at varying times since host

548   colonization. *Evol. Lett.* **3**, 555–566 (2019).

549   37.   Kubisch, A., Holt, R. D., Poethke, H. J. & Fronhofer, E. A. Where am I and why?

550   Synthesizing range biology and the eco-evolutionary dynamics of dispersal. *Oikos* **123**,

551   5–22 (2014).

552   38.   Dunn, A. M. & Hatcher, M. J. Parasites and biological invasions: Parallels,

553   interactions, and control. *Trends Parasitol.* **31**, 189–199 (2015).

554   39.   Brockhurst, M. A. & Koskella, B. Experimental coevolution of species interactions.

555   *Trends Ecol. Evol.* **28**, 367–375 (2013).

556   40.   Boots, M. & Mealor, M. Local interactions select for lower pathogen infectivity.

557   *Science (80-.).* **315**, 1284–1286 (2007).

558   41.   Kerr, B., Neuhauser, C., Bohannan, B. J. M. & Dean, A. M. Local migration promotes

559   competitive restraint in a host-pathogen 'tragedy of the commons'. *Nature* **442**, 75–78

560   (2006).

561   42.   Berngruber, T. W., Lion, S. & Gandon, S. Spatial structure, transmission modes and

562   the evolution of viral exploitation strategies. *PLoS Pathog.* **11**, e1004810 (2015).

563   43.   Boots, M. & Sasaki, A. 'Small worlds' and the evolution of virulence: infection occurs

564   locally and at a distance. *Proc. R. Soc. B-Biological Sci.* **266**, 1933–1938 (1999).

565   44.   Yin, J. Evolution of bacteriophage T7 in a growing plaque. *J. Bacteriol.* **175**, 1272–

566   1277 (1993).

567   45.   Friedenberg, N. A. Experimental evolution of dispersal in spatiotemporally variable

568   microcosms. *Ecol. Lett.* **6**, 953–959 (2003).

569   46.   Ochocki, B. M. & Miller, T. E. X. Rapid evolution of dispersal ability makes biological

570   invasions faster and more variable. *Nat. Commun.* **8**, 1–8 (2017).

571   47.   Fronhofer, E. A. & Altermatt, F. Eco-evolutionary feedbacks during experimental

572   range expansions. *Nat. Commun.* **6**, 6844 (2015).

573   48.   Lion, S., Van Baalen, M. & Wilson, W. G. The evolution of parasite manipulation of

574   host dispersal. *Proc. R. Soc. B Biol. Sci.* **273**, 1063–1071 (2006).

575   49.   Thieme, H. R. *Mathematics in population biology*. (Princeton University Press, 2018).

576   50.   Zilio, G. *et al.* Travelling with a prasite: the evolution of resistance and dispersal

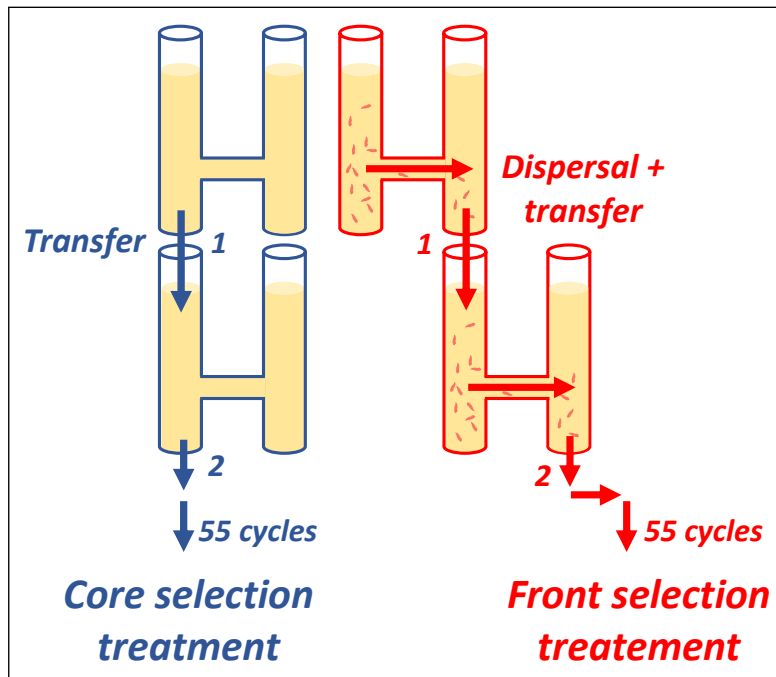577   syndrome dyring experimental range expansion. *BioXriv* (2020)

578   doi:http://dx.doi.org/10.1101/2020.01.29.924498.

579   51.   Pérez-Tris, J. & Bensch, S. Dispersal increases local transmission of avian malarial

580   parasites. *Ecol. Lett.* **8**, 838–845 (2005).

581   52.   Nidelet, T., Koella, J. C. & Kaltz, O. Effects of shortened host life span on the

582   evolution of parasite life history and virulence in a microbial host-parasite system.

583   *BMC Evol. Biol.* **9**, 1–10 (2009).

584   53.   Magalon, H., Nidelet, T., Martin, G. & Kaltz, O. Host growth conditions influence

585   experimental evolution of life history and virulence of a parasite with vertical and

586   horizontal transmission. *Evolution (N. Y).* **64**, 2126–2138 (2010).

587   54.   Restif, O. & Kaltz, O. Condition-dependent virulence in a horizontally and vertically

588   transmitted bacterial parasite. *Oikos* **114**, 148–158 (2006).

589   55.   Moore, J. *Parasites and the behaviour of animals. Oxford series in ecology and*

590   *evolution* (Oxford University Press, 2002).

591   56.   Martini, X., Hoffmann, M., Coy, M. R., Stelinski, L. L. & Pelz-Stelinski, K. S.

592   Infection of an insect vector with a bacterial plant pathogen increases its propensity for

593   dispersal. *PLoS One* **10**, 1–16 (2015).

594   57.   Fellous, S., Quillery, E., Duncan, A. B. & Kaltz, O. Parasitic infection reduces

595   dispersal of ciliate host. *Biol. Lett.* **7**, 327–329 (2011).

596   58.   Nørgaard, L. S., Phillips, B. L. & Hall, M. D. Can pathogens optimize both

597   transmission and dispersal by exploiting sexual dimorphism in their hosts? *Biol. Lett.*

598   **15**, 20190180 (2019).

599   59.   Bradley, C. A. & Altizer, S. Parasites hinder monarch butterfly flight: Implications for

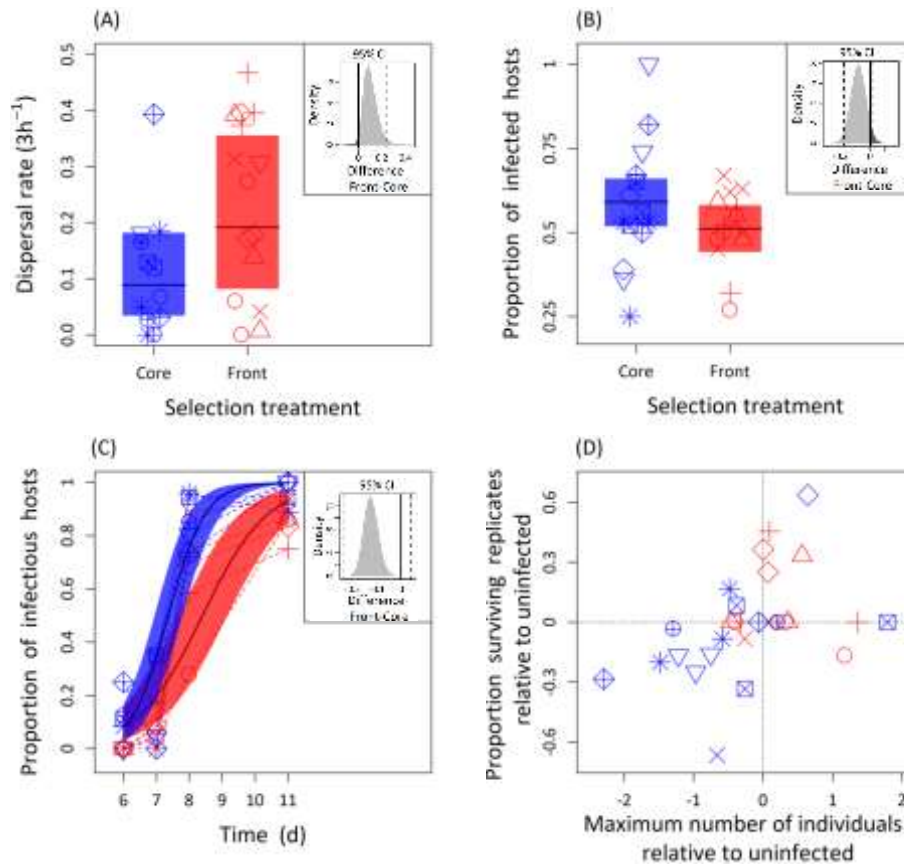600   disease spread in migratory hosts. *Ecol. Lett.* **8**, 290–300 (2005).

601   60.   Goodacre, S. L. *et al.* Microbial modification of host long-distance dispersal capacity.

602   *BMC Biol.* **7**, (2009).

603   61.   Fels, D., Vignon, M. & Kaltz, O. Ecological and genetic determinants of multiple

604   infection and aggregation in a microbial host-parasite system. *Parasitology* **135**, 1373–

605   1383 (2008).

606   62.   Bauer, A., Haine, E. R., Perrot-Minnot, M. J. & Rigaud, T. The acanthocephalan

607   parasite Polymorphus minutus alters the geotactic and clinging behaviours of two

608   sympatric amphipod hosts: The native Gammarus pulex and the invasive Gammarus

609   roeseli. *J. Zool.* **267**, 39–43 (2005).

610   63.   Lion, S. & Boots, M. Are parasites '"prudent"' in space? *Ecol. Lett.* **13**, 1245–1255

611   (2010).

612   64.   Kaltz, O., Koella, J. C., Evolutive, L. D. P., Pierre, U. & Bernard, S. Host growth

613   conditions regulate the plasticity of horizontal and vertical transmission in Holospora

614   undulata, a bacterial parasite of the protozoan Paramecium caudatum. *Evolution (N. Y).*

615   **57**, 1535–1542 (2003).

616   65.   Burton, O. J., Phillips, B. L. & Travis, J. M. J. Trade-offs and the evolution of life-

617   histories during range expansion. *Ecol. Lett.* **13**, 1210–1220 (2010).

618   66.   Ebert, D. The epidemiology and evolution of symbionts with mixed-mode

619   transmission. *Annu. Rev. Ecol. Evol. Syst.* **44**, 623–643 (2013).

620   67.   Su, M., Chen, G. & Yang, Y. Dynamics of host-parasite interactions with horizontal

621   and vertical transmissions in spatially heterogeneous environment. *Phys. A Stat. Mech.*

622   *its Appl.* **517**, 452–458 (2019).

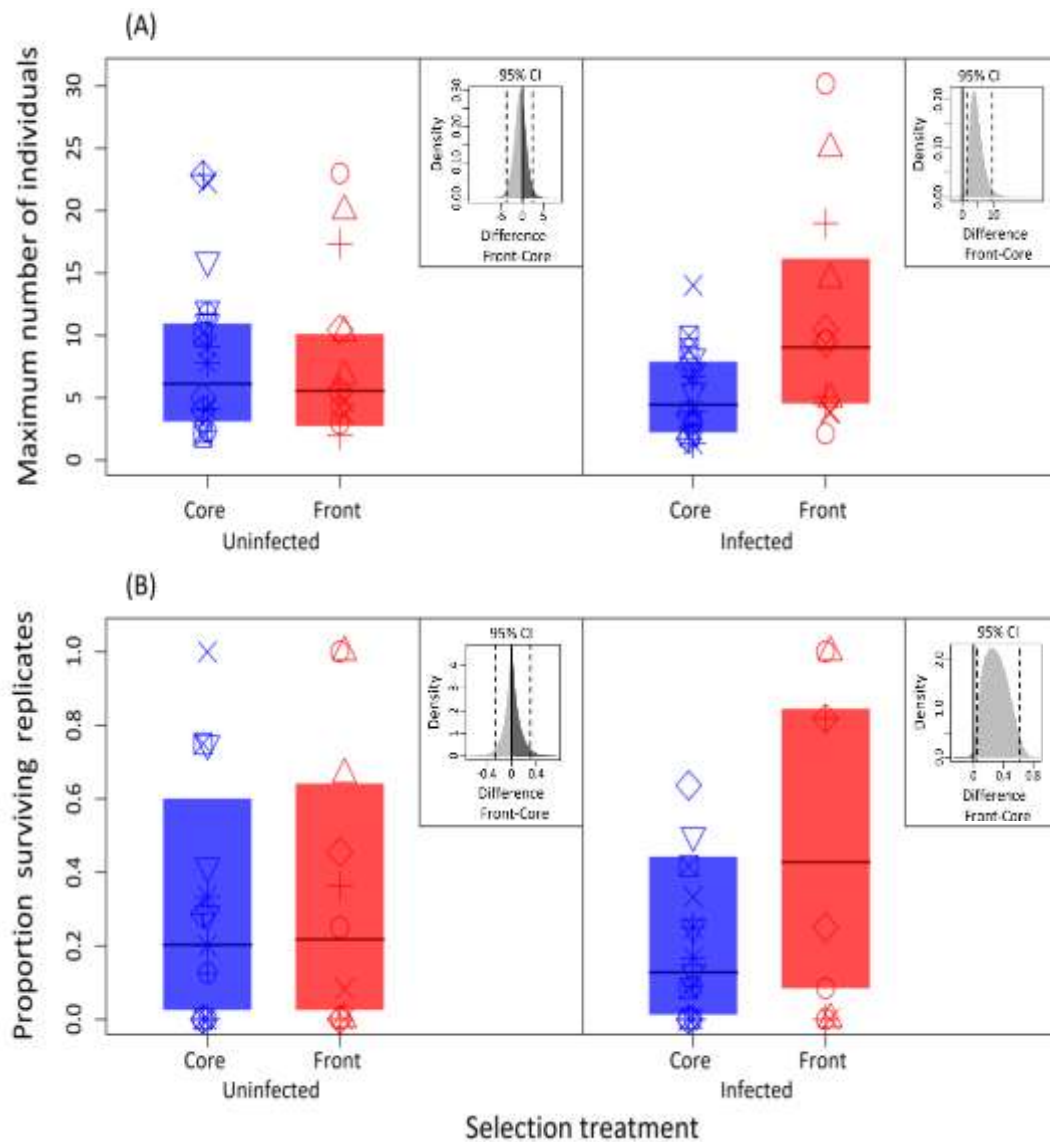623   68.   Wichterman, R. *The biology of Paramecium.* (Plenum Press, New York, 1986).

624   69. Nidelet, T. & Kaltz, O. Direct and correlated responses to selection in a host-parasite

625   system: Testing for the emergence of genotype specificity. *Evolution (N. Y).* **61**, 1803–

626   1811 (2007).

627   70. Görtz, H. D. & Dieckmann, J. Life cycle and infectivity of Holospora elegans

628   Haffkine, a micronucleus-specific symbiont of Paramecium caudatum (Ehrenberg).

629   *Protistologia* **16**, 591–603 (1980).

630   71. Fokin, S. I. & Görtz, H.-D. Diversity of Holospora bacteria in Paramecium and their

631   characterization. in *Endosymbionts in Paramecium* 162–194 (2009).

632   doi:10.1016/j.ejop.2011.10.002.

633   72. Pennekamp, F., Schtickzelle, N. & Petchey, O. L. BEMOVI, software for extracting

634   behavior and morphology from videos, illustrated with analyses of microbes. *Ecol.*

635   *Evol.* **5**, 2584–2595 (2015).

636   73. Bates, D., Machler, M., Bolker, B. M. & Walker, S. C. Fitting linear mixed-effect

637   models using lme4. *J. Stat. Softw.* (2015).

638   74. Fox, J. & Weisberg, S. *An R companion to applied regression.* (SAGE Publication Inc.,

639   2018).

640   75. Fronhofer, E. A. *et al.* Bottom-up and top-down control of dispersal across major

641   organismal groups: a coordinated distributed experiment. *Nat. Ecol. Evol.* 213256

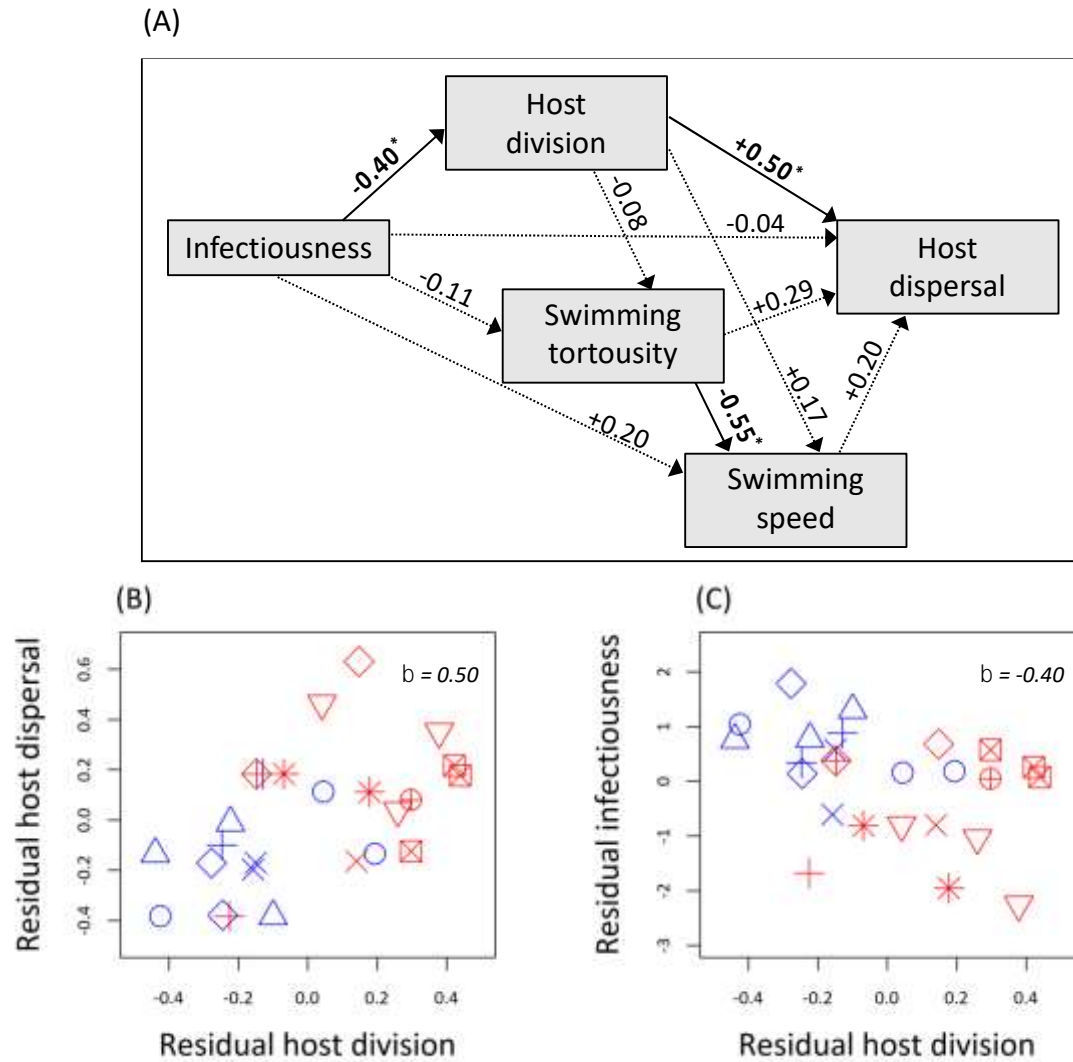642   (2017) doi:10.1101/213256.

643

644

Fig. 1. Experimental design of the long-term selection experiment, using 2-patch dispersal systems. Infected populations were placed in the 'core' tube and allowed to disperse to the other 'front' tube during 3 h (horizontal arrows). In the front selection treatment (red), only the dispersing fraction of the population was maintained, whereas in the core selection treatment (blue) only the non-dispersing fraction was maintained. After adjustment of initial densities, the selected fractions were then transferred to a new tube (vertical arrows) and grown for 1 week, during which time demographic and epidemiological processes acted freely. A total of 55 dispersal/growth cycles were performed, for 5 core and 5 front selection lines.
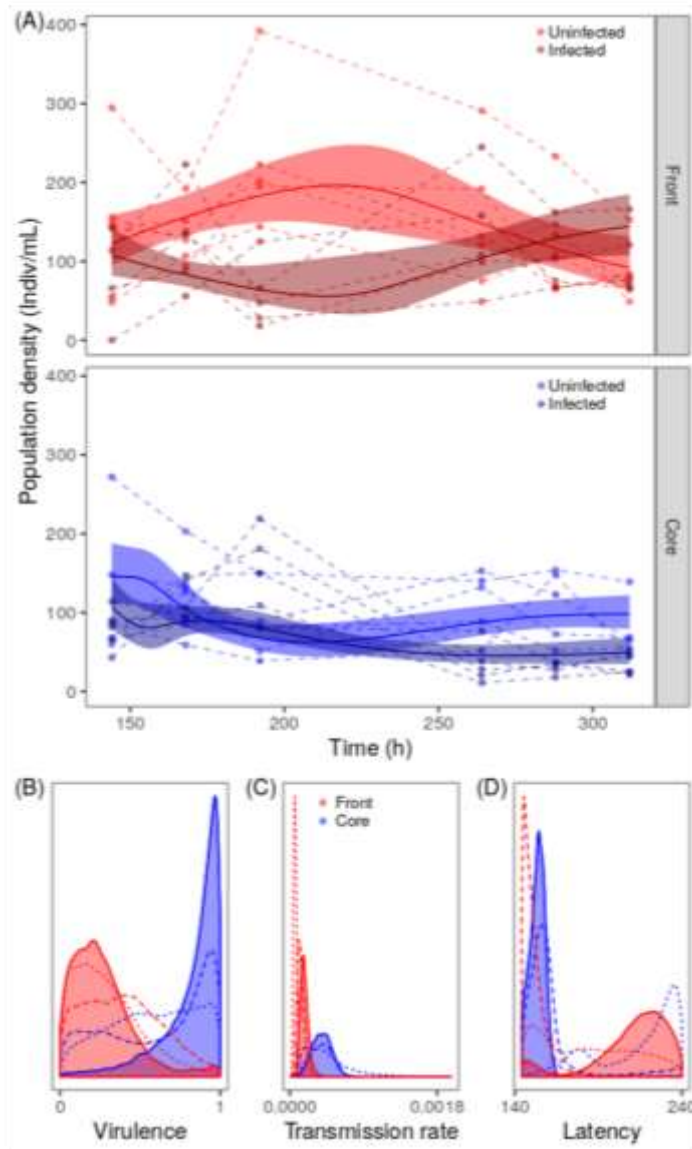
654

Fig. 2. Dispersal and infection life-cycle traits of evolved parasites from core selection (blue) and front selection (red) treatments, measured on naïve *Paramecium*. **(A) Dispersal rate**. Proportion of dispersing infected hosts observed in infected assay cultures placed for 3 h in a dispersal system. **(B) Infectivity.** Proportion of infected hosts in assay cultures on day 4 post-inoculation (p.i.). **(C) Infectiousness**. Proportion of infectious hosts in infected assay cultures between day 6 and 11 p.i.. Infectious hosts are individuals that produce infective spores of the parasite. **(D) Virulence.** Association between infected host division and survival, expressed relative to uninfected hosts (infected minus uninfected). Negative values indicate negative effects of infection on the host trait. Panels (A)-(C) show means and 95 % confidence intervals of the model predictions. Small insert panels show predictive distributions (and 95% CI) of the difference between front and core treatments. Symbols represent observed means for different combinations of parasite selection line and assay host genotype. Different symbols refer to different parasite selection lines (n = 10).

28

Fig. 3. Estimates of virulence of evolved parasites from core selection (blue) and front selection (red) treatments, measured on naïve *Paramecium*. **(A) Host division**. Maximum cell density of infected and uninfected *Paramecium*, as determined in a singleton assay. **(B) Host survival.** Proportion of surviving infected and uninfected replicates on day 20 in the singleton assay. All panels show means and 95 % confidence (CI) intervals of the model predictions. Small insert panels show predictive distributions (and 95% CI) of the difference between front and core treatments. Symbols represent observed means for different combinations of parasite selection line and assay host genotype. Different symbols refer to different parasite selection lines (n = 10).

Fig. 4. Relationships between parasite traits. **(A)** Path analysis testing direct and indirect effects of 4 parasite traits on infected host dispersal: (i) Infectiousness (cumulative proportion of host producing infective spores; area under the curve: day 6 - 11 p.i.); (ii) Host division (maximum infected cell density); (iii) Swimming tortuosity ($\approx$ trajectory changes) and (iv) net swimming speed of infected singletons. Analysis based on trait means for different combinations of parasite selection line and host assay genotype ($n = 25$) and performed on residuals, after correcting for overall effects of host assay genotype. Standardised beta regression coefficients (β) are shown above arrows ($^*p < 0.05$); **(B)** Relationship between residual host division and dispersal; **(C)** Relationship between residual horizontal transmission investment and host division.

Fig. 5. Fit of the epidemiological model. **(A)** Fit of the epidemiological model (equations 6-8) to infected and uninfected host density time-series data, obtained for assay cultures infected with core (blue) and front (red) parasites. Curve fits shown for host genotype 63D (for other genotypes, see Fig. S11). Dashed lines represent observed densities for different replicate assay cultures, solid lines and shaded areas represent posterior model predictions (mean and 95% CI). **(B)-(D)** Posterior distributions for virulence (= reduction in host division rate), horizontal transmission rate and latency, respectively. Solid lines and shaded areas show posterior distributions for host genotype 63D, dashed lines for host genotype C173, and the dotted lines for genotype C023.